J Neurophysiol 93: 1659–1670, 2005;
doi:10.1152/jn.01213.2003.

Visuotopic Mapping Through a Multichannel Stimulating Implant in Primate V1

D. C. Bradley,[1] P. R. Troyk,[5] J. A. Berg,[1] M. Bak,[7] S. Cogan,[8] R. Erickson,[3] C. Kufta, M. Mascaro,[4] D. McCreery,[6] E. M. Schmidt, V. L. Towle,[2] and H. Xu[1]

[1]*Departments of Psychology,* [2]*Neurology,* [3]*Neurosurgery, and* [4]*Statistics, University of Chicago, Chicago, Illinois;* [5]*Pritzker Institute of Biomedical Science and Engineering, Illinois Institute of Technology, Chicago, Illinois;* [6]*Huntington Medical Research Institute, Pasadena, California;* [7]*Laboratory of Neural Control, National Institutes of Health, Bethesda, Maryland; and* [8]*EIC Laboratories, Norwood, Massachusetts*

Submitted 15 December 2003; accepted in final form 19 August 2004

Bradley, D. C., P. R. Troyk, J. A. Berg, M. Bak, S. Cogan, R. Erickson, C. Kufta, M. Mascaro, D. McCreery, E. M. Schmidt, V. L. Towle, and H. Xu. Visuotopic mapping through a multichannel stimulating implant in primate V1. *J Neurophysiol* 93: 1659–1670, 2005; doi:10.1152/jn.01213.2003. We report on our efforts to establish an animal model for the development and testing of a cortical visual prostheses. One-hundred-fifty-two electrodes were implanted in the primary visual cortex of a rhesus monkey. The electrodes were made from iridium with an activated iridium oxide film, which has a large charge capacity for a given surface area, and insulated with parylene-C. One-hundred-fourteen electrodes were functional after implantation. The activity of small (2–3) neuronal clusters was first recorded to map the visually responsive region corresponding to each electrode. The animal was then trained in a memory (delayed) saccade task, first with a visual target, then to a target defined by direct cortical stimulation with coordinates specified by the stimulating electrode's mapped receptive field. The SD of saccade endpoints was ~2.5 larger for electrically stimulated versus visual saccades; nevertheless, when trial-to-trial scatter was averaged out, the correlation between saccade end points and receptive field locations was highly significant and approached unity after several months of training. Five electrodes were left unused until the monkey was fully trained; when these were introduced, the receptive field-saccade correlations were high on the first day of use ($R = 0.85$, $P = 0.03$ for angle, $R = 0.98$, $P < 0.001$ for eccentricity), indicating that the monkey had not learned to perform the task empirically by memorizing reward zones. The results of this experiment suggest the potential for rigorous behavioral testing of cortical visual prostheses in the macaque.

INTRODUCTION

Most instances of new blindness are caused by problems with the eye or the optic nerve, and in most cases, the visual cortex is probably intact (Ferree 1966). This suggests the enormous potential of an intracortical prosthesis, an electrode array that in theory stimulates cortical neurons in such a way as to construct a visual experience. Experiments dating back to 1918 have shown that on electrical stimulation of the primary visual cortex, humans experience sensations, known as phosphenes, which are spatially localized and occasionally have colors and the appearance of depth. But despite reports in the popular press, even the largest-scale experiments of this kind have failed to produce anything resembling functional vision (Brindley and Lewin 1968; Dobelle 2000; Dobelle and Mladejovsky 1974; Dobelle et al. 1974, 1976; Schmidt et al. 1996).

Figure 1 shows three renditions of a face, the first (*A*) in grayscale at high resolution, the second (*B*) in grayscale at medium resolution, and the third (*C*) in black and white at low resolution. At the moment, *B* would be quite hopeful, even projecting ahead many years, as it would imply an array of 1,152 electrodes, evenly spaced, each capable of inducing 1 of 255 levels of gray perception. At present, we do not know how to modulate the perception of gray. *C,* which has a resolution of 72 pixels, is commensurate with the largest implants to date. It is unrecognizable. Thus it is clear that a great deal of progress needs to be made in visual prosthesis technology.

Unfortunately, little progress is being made. The handful of volunteers for intracortical implants can only provide so much information, not just because they are few, but because they can only spend so much time doing experiments. Obviously, invasive procedures other than the implant itself are out of the question. So there is a pressing need for animal models in prosthesis development.

It has been our goal to develop such a model. The main issues we have addressed up to now are how to construct a durable and safe electrode array, how to implant and interface with this array, and how to evaluate the perceptual effects of stimulation through the array. In this report, we describe progress in all three areas with emphasis on the latter.

Portions of these results have been reported briefly elsewhere (Troyk et al. 2003).

METHODS

In overview, 152 electrodes were implanted in the right primary visual cortex (V1) of a 5-yr-old, 7-kg male rhesus monkey. After implantation, recordings of neuronal activities were made to find the visually responsive region for each electrode channel, and the monkey was trained to make eye movements to these locations on stimulation of the corresponding channels. The animal was killed 16 mo after implantation and histology carried out to examine the integrity of cortical tissue under the implant.

Electrodes

The initial array contained 192 electrodes: 128 were fabricated at the Huntington Medical Research Institute (HMRI), the remaining 64

Address for reprint requests and other correspondence: D. Bradley, Dept. of Psychology, University of Chicago, 5848 S. University Ave., Green 314, Chicago, IL 60637 (E-mail: bradley@uchicago.edu).

The costs of publication of this article were defrayed in part by the payment of page charges. The article must therefore be hereby marked "*advertisement*" in accordance with 18 U.S.C. Section 1734 solely to indicate this fact.

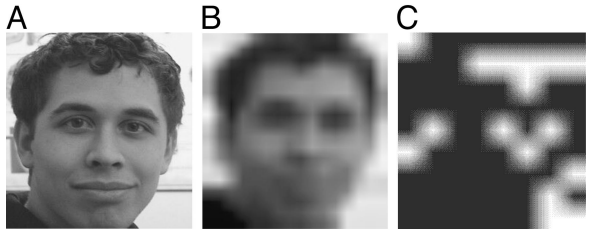

FIG. 1. Three versions of 1 image. *A*: 255 × 286 pixels, 16-bit grayscale. *B*: 32 × 36 pixels, 8-bit grayscale. *C*: 8 × 9 pixels, black and white. *C* is potentially within reach if electrodes can be spaced evenly on the cortex. *B* would require an array ~10 times larger than any every implanted and would need to manipulate brightness perception very precisely.

at the National Institutes of Health. The HMRI electrodes took the form of 8-pin clusters, whereas the National Institutes of Health (NIH) electrodes were of the "hat-pin" type used previously in humans (Bak et al. 1990). For the NIH electrodes, 37-μm iridium wire was welded to a 25-μm gold wire lead, and the joint was reinforced with a bead of biocompatible epoxy. The iridium wire was sharpened to 1–2 μm and the entire assembly coated with 3–4 μm of parylene-C insulation. Silane was used to enhance adhesion of the parylene-C. A dual-beam eximer laser was then used to expose 200–300 μm^2 of iridium at the tip of the microelectrode.

The HMRI electrodes used 35-μm iridium wire. One end of the electrode blank was etched electrolytically to a cone with an included angle of 10° and a blunt tip with a curvature radius 5–6 μm. Blunt tips minimize tissue injury and help to equalize current density over the exposed surface; this in turn reduces erosion of the metal when the electrode is subjected to long-term pulsing. An uninsulated platinum lead wire was microwelded to the shaft ~1.5 mm above the tip. The electrode was coated with 2.5 μm parylene-C after application of adhesion-enhancing silane. The parylene-C was then ablated from the tip with an eximer laser. The electrode's active geometric surface area was 500 ± 100 μm. (Fig. 2)

These electrodes were then assembled into clusters of eight. A mold was used to hold the tips of the electrodes in separate alignment tubes, 500 μm apart. The mold cavity was filled with casting epoxy (EpoTek 301, Epoxy Technology) to form the cluster's superstructure. The platinum leads were coiled around a segment of silicone rubber tubing, 0.5 mm in diameter, and coated with type A silicone to form a flexible cable ~15 cm in length. After extrusion from the mold, electrodes were activated (oxidized) using a protocol developed at EIC (Cambridge, MA) to increase their charge capacity.

The NIH electrodes were all 1.5 mm in length, whereas the HMRI electrodes were staggered within each cluster to have lengths of 0.7, 0.9, and 1.3 mm. The latter was done because we did not know a priori which lengths would be effective, so we chose to introduce some variance. This probably combined with significant variance due to changes in tip depth over time. There was no appreciable difference in the precision of stimulated saccades for the different electrode lengths; therefore data were pooled across electrode lengths for analysis. Similarly, results were comparable for the HMRI versus NIH electrodes, so data were pooled across this variable as well.

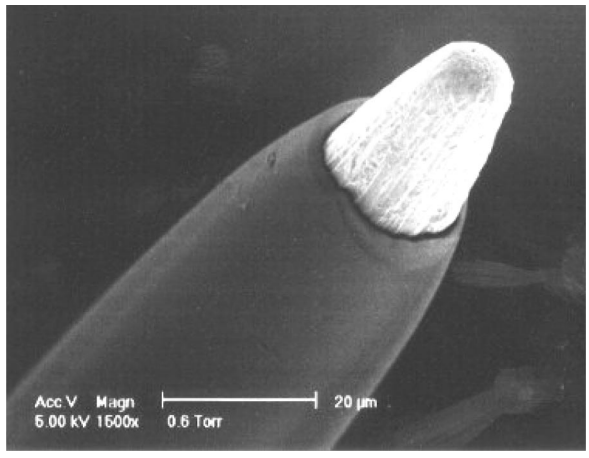

FIG. 2. Scanning electron micrograph of a Huntington Medical Research Institute (HMRI) electrode. Approximately 200 μm^2 of iridium is exposed with an excimer laser. The insulation is parylene-C.

Connectors

Custom connector banks were built with assemblies of Omnetics 0.025-in center-to-center connectors (Fig. 3). A polycarbonate housing was machined to hold one bank (NIH electrodes) or two banks (HMRI electrodes) of connectors. The outer dimensions of the housings were 1.2 × 2.1 × 2.5 and 1.2 × 1.2 × 2.5 cm for the NIH and HMRI electrode banks, respectively. The connectors were glued inside the housing with epoxy, which formed a water-resistant seal. When connectors were not in use, a cap was screwed down onto the housing with an O-ring seal to prevent liquid from leaking into the connectors.

Stimulator design and construction

We used a bench-top model of a 128-channel implantable stimulator developed at the Illinois Institute of Technology. The device provides up to 128 channels of biphasic, charge-balanced stimulation to intracortical microelectrodes. Arbitrary stimulation trains are defined off-line with a high-level graphical user interface, and the PC uploads instructions to the stimulator microprocessor via a high-speed customized interface.

Functionally, the stimulator is divided into a digital command and control section, and custom designed integrated circuits known as block chips. Each block chip outputs to eight microelectrodes and receives serial digital data that specify the amplitude and pulse width for each of its eight electrodes. The command and control section provided the interface to the PC and allowed for the specification of a stimulus pulse each 6.4 μs for each 1-s command stream.

Surgical techniques

Preoperative CT and MRI scans were taken, and the data were used to fabricate scale-replica plastic models of the brain and skull. These

FIG. 3. Single-row connector bank; dual-row assemblies were also made. The housing was machined from polycarbonate with grooves to hold 10-pin, 0.025-in center Omnetics connectors, sealed in with epoxy. A polycarbonate cover was secured with screws, with an O-ring in between to make a water resistant seal. The Omnetics connectors are visible through the cover. The epoxy around the connectors prevented moisture from seeping up from underneath. The connector assembly is shown mounted to the acrylic skull cap.

models were used to estimate electrode lead lengths, tolerable connector sizes, anchor screw positions, and craniotomy boundaries. The imaging data were also used as controls for postoperative images.

In surgery, a craniotomy was performed to expose the lateral surface of the right occipital cortex, from the superior sagittal sinus medially to the transverse sinus laterally. A sterile template, with dimensions determined using the plastic models, was used to guide placement of the craniotomy and connector sites. The dura was opened, and microelectrode placement sites were identified on the cortical surface. At this point the connectors, with electrodes preattached, were mounted to the skull with titanium screws. Custom-made, polycarbonate comb-like structures were used to guide the electrode lead cables toward the cortical insertion sites (Fig. 4). Hat-pin electrodes were inserted manually (with forceps), whereas the eight-electrode clusters were inserted at 1 m/s with a pneumatic device. All electrodes were placed in the V1 operculum. Once all of the electrodes were inserted and their locations photodocumented, a free flap of fascia from temporalis muscle was placed over the craniotomy site, covering the entire dural opening. The bone flap was replaced and the entire operative site was filled with acrylic, incorporating all elements of implanted hardware. The surgery lasted 8.5 h.

Training

The monkey was trained in a memory saccade task that involved a period of fixation, during which either a visual target was flashed or a cortical site was directly stimulated, followed by a saccade to the remembered location of the target. While a task involving the immediate saccade to a target would have been faster, it was necessary to use a memory saccade task to avoid confusing the animal. Normally, when the eyes move, the displacement of visual objects on the retina is perceptually compensated; because of this, human patients who move their eyes during cortical stimulation report that the phosphene is moving—the compensation occurs where it is not needed (Schmidt et al. 1996). One obviates this problem by requiring the monkey to saccade to a remembered location after the stimulus is extinguished.

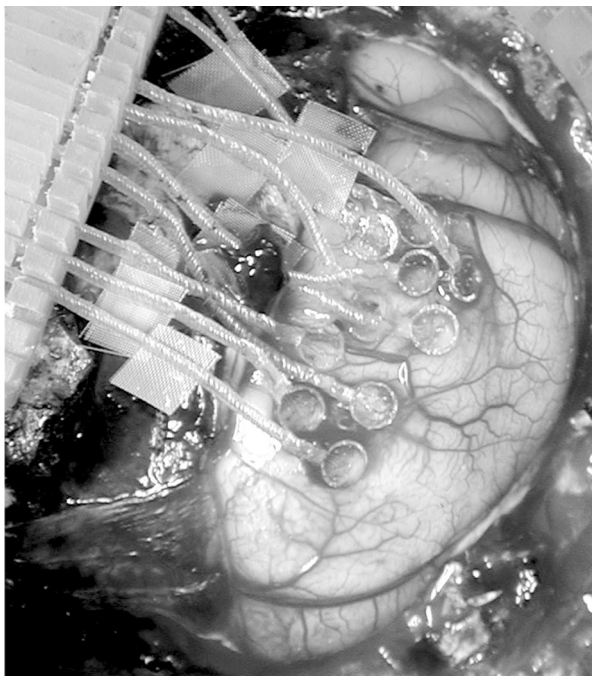

FIG. 4. Placement of the 8-electrode clusters during surgery. Each ring is a wire loop encompassing a group of 8 evenly spaced electrodes; these are inserted at high speed with a pneumatic device. Care was taken to avoid placing an electrode cluster on major vasculature; single hat-pin electrodes (not shown) were used to fill in the gaps. The rectangular objects are Teflon pads glued to the electrode leads. These settle on wet tissue and adhere by capillary action, providing stability to the electrodes during surgery. The large white structure in the upper left is a custom-made comb used to guide the electrode leads. It was made beforehand using a scale-replica skull model. Without this comb, the tension of the electrode leads tends to displace them from their site of insertion. The comb was hinged so it could be removed before pouring on the acrylic skull cap.

In initial training, the monkey sat in a dark chamber and fixated for 1.5 s, during which a small visual target was flashed for 100 ms at a random location in the left visual field (0.01° diam, 42 cd/m^2). The locations of the visual targets bore no relationship to the locations of the targets during electrically stimulated trials. After the fixation point disappeared the monkey was required to saccade to the flashed location. Fluid rewards were given when the saccade was within 0.25–2.5° of the target. Once the monkey had learned the task, the visual flash was replaced with a 1-s (initially) or 0.2-s (later) cortical stimulation period. In all cases, $\geq$0.5 s elapsed between the current offset and the extinction of the fixation point (and thus the initiation of the saccade). This gap was imposed to allow any perceptual persistence to fade completely. For the 1-s duration stimulus, we used 200-ms pulse trains separated by 200 ms off times such that there were three 200-ms pulse trains for each 1-s stimulation. Stimulation was 200-Hz, biphasic, 200-μs pulses, cathodic first. For the HMRI electrodes, constant current stimulation was at 20–25 μA ($\sim$1 mC/cm^2). For the NIH electrodes, constant current stimulation was at 12–13 μA ($\sim$1.25 mC/cm^2).

Electrophysiology

By "receptive fields," we will mean the visually responsive regions mapped at the various recording channels. Several approaches were taken to map these fields. We began by mapping qualitatively, using a hand-held computer mouse to displace a small dot pattern on a CRT display 57 cm from the monkey's eyes. On 68/114 channels, a receptive field could be qualitatively identified, and the majority of these fields lay within a 10 $\times$ 10° region left of and mainly below the fixation point. We then mapped this region more systematically, first using 1° flicker patterns at 0.5° spacing, then 2° random-line patterns, 1° spacing, moving at 3°/s in one of eight directions {0, 45, . . ., 315°}. The random-line patterns are the one-dimensional equivalent of random dot patterns.

Recordings were made through 96 parallel channels using a Plexon Multichannel Acquisition Processor. For each channel, time-voltage acceptance windows were adjusted so that the total baseline firing rate was $\sim$20–30 spikes/s, corresponding to roughly two to three neurons. Off-line, data were z scored so that they could be pooled across sessions while preserving inter-channel response differences.

Histology

The monkey was anesthetized with pentobarbital and perfused through the ascending aorta with a saline prewash followed by 2 l of half-strength Karnovsky's fixative. The head was removed and post-fixed in the same solution for 4 days. The microelectrodes and clusters of microelectrodes were resected from the vestment of connective tissue and removed from the brain. The portion of the visual cortex containing most of the electrodes was resected as a single block and embedded into paraffin. The tissue was sectioned at a thickness of 6 μm in the plane perpendicular to the pia (approximately parallel to the electrode shafts) and stained with cresyl violet (Nissl stain).

RESULTS

Integrity and electrical properties of the implant

Due to manufacturing problems, only 152 of the original 192 electrodes were implanted, and 38 of these had connector

problems that were known prior to surgery. Therefore 114 functional electrodes were implanted.

The small-signal (50-mV excitation) impedance of the implanted electrodes at 1 kHz varied from 80 kΩ to 1.6 MΩ and averaged 560 kΩ. This value may seem small for recording—single-electrode recordings are commonly done with impedances in the megaohm range—but activated iridium has a large charge capacity that results in low impedance for a given area of exposed metallic surface. For a given surface area, the low impedance does not hinder but rather facilitates recording by boosting the signal to noise ratio. The impedance of activated iridium can be further reduced by placing an anodic bias (~0.4–0.8 V) on the electrode. However, because this was our first implanted animal, we did not use anodic bias out of concern for maintaining the long-term integrity of the electrodes.

Figure 5 shows a voltage-time trace for two electrodes, A and B, driven with a 20-μA biphasic constant current waveform. These two electrodes show the extremes of behavior for the 114 implanted electrodes and are representative of the electrode population. The waveform for electrode A shows an access resistance of ~37.5 kΩ and an equivalent electrode capacitance of ~5 nF. In contrast, the waveform for electrode B displays an access resistance of ~87.5 kΩ, and an equivalent electrode capacitance of ~2.5 nF. At this stimulus level, the deliverable charge density for both electrodes was 0.4 mC/cm^2, a modest charge density for iridium oxide. However, electrode B shows a larger voltage drop with a distinctive change in slope near the cathodic peak. Undoubtedly, this undesired voltage excursion was a result of our not using anodic bias for the electrodes. Because these waveforms were taken near the end of the 16-mo implantation study, we can feel confident that during our experimental period the electrodes were capable of delivering an adequate electrical stimulus. In future studies we will optimize charge capacity by using an anodic bias. Despite the somewhat excessive voltage excursions for some of the electrodes, we demonstrate below that these characteristics were sufficient for our goal of using the same electrode array to record from and stimulate cortical neurons.

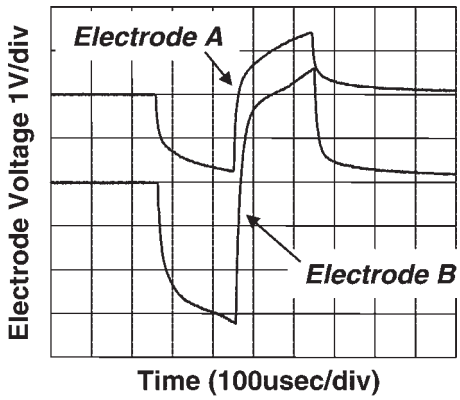

FIG. 5. Voltage waveforms for 2 representative electrodes in response to a symmetric biphasic constant-current stimulus of 20 μA and 200 μs per phase. Electrode A shows an access resistance of 37.5 kΩ and charging of the electrode capacitance that is near the generally regarded safe limit of −0.6V with respect to Ag AgCl. Electrode B shows an access resistance of 87.5 kΩ and a cathodic voltage excursion that is beyond the safe limit. However, both electrodes were able to deliver an adequate stimulus and serve as recording electrodes for the duration of the 16-mo study.

Receptive field mapping

In initial mapping with a hand-driven stimulus, the majority of visually responsive locations were confined to a 10 × 10° region contained largely in the lower left visual quadrant. We therefore used 1° flicker patterns at 0.5° spacing to map this region more systematically. Recall from METHODS that for each channel, roughly two to three neurons were recorded simultaneously and that by receptive field we mean the visual region to which this multiunit sample was responsive. Visual response data (firing rates) for 114 channels were fit with a sliding two-dimensional (2D) Gaussian (whether or not a receptive field was apparent) to estimate the midpoint and the tuning width of the receptive field but fits only converged for 56 of the channels. The median tuning width (SD of the Gaussian) for these was 0.71 ± 0.01°, and the mean ratio of width to eccentricity was 0.11 ± 0.01°. Thus for example, a channel the RF center of which was 5° from the fovea would have a tuning width of 0.55°. Because this is roughly the size of V1 fields at similar eccentricities (Hubel and Wiesel 1968) and because our estimates of receptive field width are likely overestimated due to the coarse resolution imposed by the 0.5° stimuli, our electrodes were probably recording from cell clusters on a scale not larger than the hypercolumn.

We then mapped the same 10 × 10° area with moving random-line stimuli. In this case the stimuli were 2° wide and spaced at 1° intervals. This is actually a three-dimensional map containing 800 locations (100 positions by 8 directions) but the angles were collapsed to find the 2D receptive fields. Because responses were in the form of z scores (within a given channel, but pooled across sessions), we said that a given channel had a significant receptive field if it contained an adjacent pair of responses both >2.0. Thirty-three channels met this requirement, and they are all shown in Fig. 6. Note that the RFs appear large but this is due to the large stimuli. Also, because a number of the RFs in evidence are at the boundaries, it is likely that a number of channels had RFs outside the test region.

Direction and orientation tuning

For each of the 33 channels with a significant RF, we tested for orientation and direction tuning with an ANOVA. At the 95% confidence level, 7/33 channels (21%) were directional and 11/33 channels (33%) were orientation selective. The number of neurons with either direction tuning, orientation tuning or both was 13 (39%). An example of directional tuning is shown in Fig. 7. Bear in mind that these data correspond to multiunit samples so we do not expect tuning properties to be as sharp as those for single-neuron recordings.

Saccade-to-phosphene task

The monkey was initially trained in a memory saccade task using visual targets. We then started to interleave saccade-to-flash and saccade-to-phosphene task blocks, where within a given block, only one type of stimulus was shown; that is, visual and electrical stimuli were not interleaved trial-to-trial. Even when the monkey was well trained in the phosphene task, we continued to interleave blocks of the visual stimuli to compare visually and electrically stimulated performance.

A subset of the 114 functional channels was used for stimulation in the saccade-to-phosphene task. We first visually

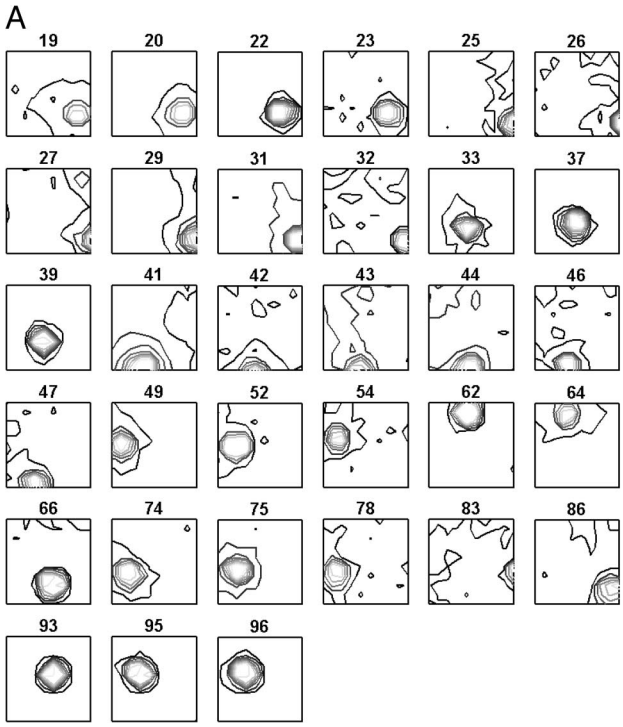

FIG. 6. *A*: receptive field maps expressed as contour plots for 33 channels that met our significance criterion (see text). The mapping stimuli were 2° in diameter so these receptive fields are overestimated in size; our concern here was to demonstrate that they were detectable. The scale on each graph is (in degrees, relative to fovea) x: −8 to 1; y: −7 to +2. Channel numbers are shown above the graphs. *B*: the locations of the electrodes (by channel number) on the V1 surface. Channels ≤54 were part of 8-electrode arrays; channels above 54 were of the hat-pin type, i.e., implanted singly or in pairs.

identified the 48 most salient receptive fields based on mapping with the 1° flicker stimuli, then randomly selected a subset of 33 of these, reserving the remaining 15 for future use.

Metrics of performance

SCATTER OF END POINTS. We computed the SD for each group of saccade end points corresponding to a given channel for all data collected in the last 5 mo of the experiment. This was done separately for x (horizontal) and y (vertical), and for phosphene versus visual targets (Table 1). As expected, there was a general tendency for the SD of end points to increase with the eccentricity of the mean end point (see slope values in Table 1). The projected SD at zero eccentricity (the intercept) was ~2.5 times larger for phosphene versus visual targets. Thus visual saccades were substantially more precise.

SPATIAL CORRELATION. From here on we will mean by "saccade" or "end point" the mean value for a given channel, averaged over trials within a given session (day). This removes trial-to-trial noise (Fig. 8) and allows us to study the animal's ability to map cortical stimulation to visual space. Stated differently, it allows us to study saccade accuracy rather than precision. For each session, we correlated the saccade end points with the receptive field centers in polar coordinates to generate two correlation coefficients, R_{angle} and R_{ecc}, where the latter corresponds to eccentricity. The angular coefficient is informative if the range of angles is not large, as in the present case.

The correlation coefficients reflect the tendency of saccades and receptive fields to vary in the same direction but do not reflect consistent misses, termed biases. Therefore we also computed the bias as the mean distance (averaged over all channels) between the receptive field centers and the saccade end points. (Multiplied by the number of end points, this becomes the Minkowski metric.)

The time course of all three statistics is plotted in Fig. 9, *left*. The graphs show three distinct periods: a first period of 3 sessions, around day 50; a second period between days 100 and 200; and a third period between days 300 and 500. The first period represents the animal's performance without any prior training. The data shown for the second period were preceded by 2 wk of daily training; unfortunately data for these 2 wk

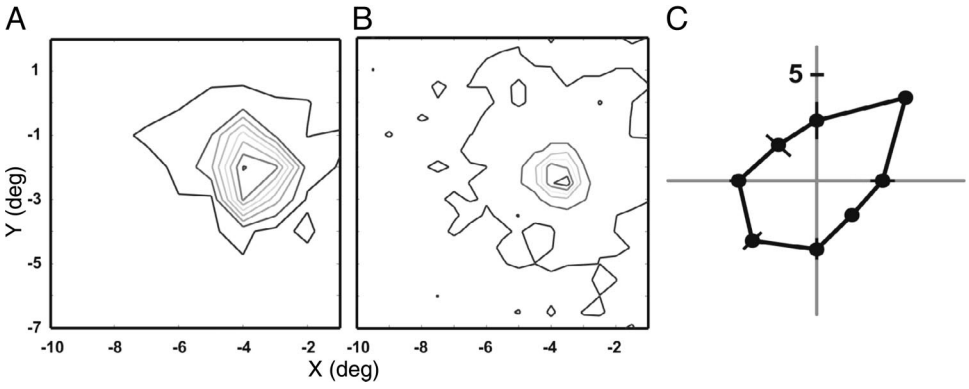

FIG. 7. Receptive field and tuning data for 1 neuron. *A*: the receptive field map using 2° oriented stimuli (as in Fig. 7). *B*: the receptive field mapped with 1° flicker stimuli. The field width is clearly narrower, though the surrounding region is somewhat noisier. This is to be expected since the wider stimulus acts as a wider band-pass (smoothing) filter. *C*: the response of the neuron, in polar coordinates, as a function of direction. Radius units are spikes/s. The cell is axis selective, preferring motion at 45 and 225°, and slightly directional, preferring 45 over 225°.

TABLE 1. *Statistics pertaining to the scatter of saccade endpoints*

	intercept	*P* (int)	Slope	*P* (slope)	Mean
Phosphene, X	1.73	0.009	0.24	0.06	2.9 ± 0.2
Phosphene, Y	1.44	0.001	0.1	0.23	1.9 ± 0.1
Visual, X	0.67	0.001	0.17	0.001	1.26 ± 0.05
Visual, Y	0.93	0.001	−0.05	0.03	0.77 ± 0.02

All numbers refer to the SD of endpoints for a given channel over the last 5 mo of the experiment.

were lost so the learning time course is unknown. The third period corresponds to sessions after a subcranial infection (see following text) and several months of inactivity.

Figure 9, *right,* shows only the data from the third period on an expanded abscissa. The animal's performance improved steadily from day 350 to day 450, ultimately reaching high levels. This is evident in the correlation coefficients (*top*), which are close to one, and the biases (*bottom*), which attain minima ~2–3°. To give a sense of scale with regard to the biases, the range of receptive field (target) eccentricities was 3.5–10°, mean 6.8°.

EMPIRICAL LEARNING. Monkeys could conceivably identify the electrode being activated by nonvisual means, then use the juice reward windows as feedback to eventually learn where to look to obtain a reward when a particular channel is stimulated. This empirical learning would obviously take time to develop.

Figure 10 shows the correlation between saccade end points and receptive fields on the first-ever day of training in the phosphene task (having previously been trained to saccade to visual targets). Both correlation coefficients were significant ($R = 0.28$, $P = 0.03$ for angle; $R = 0.30$, $P = 0.02$ for eccentricity). Because 32 different electrodes were being activated in random sequence, it is unlikely that the monkey could have worked out any correlation between electrode identity and reward zone in a matter of tens of trials per electrode.

We also introduced, near the end of the study, a group of five electrodes that had not been stimulated before. We further increased the reward window to 9° on a side, which is larger than the entire span of receptive field eccentricities, to minimize feedback pertaining to reward zones.

The "gray" (red) symbols in Fig. 9 (*right*) correspond to data from the new electrodes during the five sessions of their use. With the exception of one near-zero value in the correlation plots, all performance measures are excellent—near the optimal values obtained under any conditions—and no learning curve is apparent. For the first session when the new electrodes were introduced, the correlation coefficients were $R = 0.85$, $P = 0.03$ for angle, and $R = 0.98$, $P < 0.001$ for eccentricity. In the absence of any prior training on these channels, this argues against the possibility of empirical learning.

Trauma and retraining

Five months after array implantation, the animal became lethargic and withdrawn; within days, he was losing equilib-

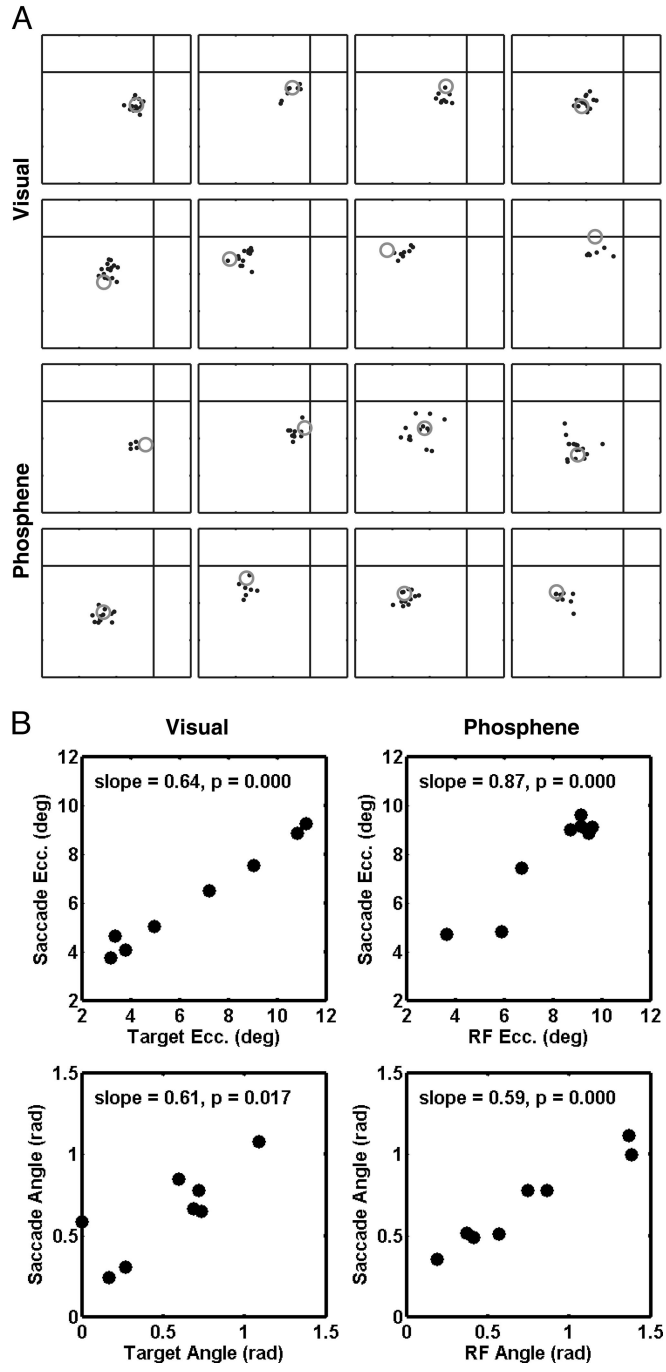

FIG. 8. Saccade endpoints for visual and phosphene tasks. *A*: 1 small circle for each saccade. The larger "gray" circle, the size of which is arbitrary, is centered on the channel's receptive field for phosphene saccades or on the visual target for visual saccades (recall that all saccades were memory saccades). Each graph spans −15 to +5° on both the horizontal and vertical axes. The monkey was fixating at (0,0), indicated by the crossed lines. Data are shown for all trials, that is, both rewarded and unrewarded, collected in a single session. One session each for visual and phosphene saccades were selected with optimal performance in mind; thus the results shown are not typical. However, for phosphene saccades, the illustrated results are representative for roughly a quarter of the electrodes in a well-trained monkey. *B*: the mean saccade endpoints, averaged over all trials of the session, compared with the visual target locations (*left*) or the channel receptive field locations (*right*). *Top*: eccentricity; *bottom*: angle. Eccentricity has units of degrees relative to the fixation point. Saccade angle is expressed in radians, where straight left is taken as 0, counterclockwise positive. For visual and phosphene targets alike, the spatial distribution of saccades is compressed, both in angular dispersion and in the range of eccentricities, as evidenced by slopes <1. Nevertheless, the relationships are in all cases significant and roughly linear, indicating that (other than compression) visuospatial information transferred through the array is undistorted. The compression is likely due to the monkey minimizing effort spent in the highly repetitive task.

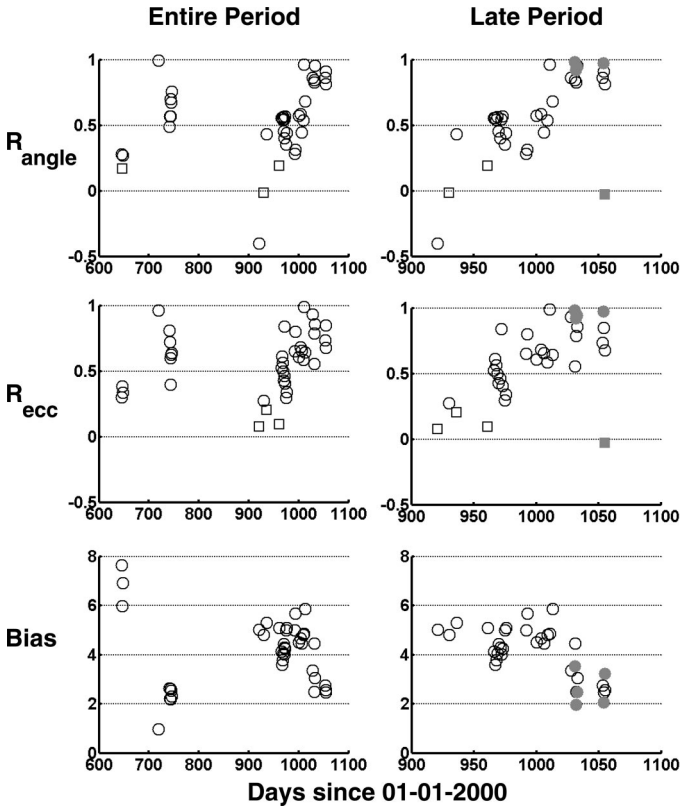

FIG. 9. Three measures of performance in the saccade-to-phosphene task, plotted over the lifetime of the animal. All quantities shown compare saccade endpoints (averaged over repeated trials for each stimulation channel) to receptive field centers. Each point represents one session and expresses a correlation or mean bias based on 32 stimulation channels and an average of 21 saccade repetitions. R_{angle} and R_{ecc} are correlation coefficients based on the angle and eccentricity of saccade vectors, respectively. Bias is the distance between the saccade endpoint and the receptive field, averaged over receptive fields (equivalently, over channels). In the *top 2 rows,* round symbols imply that R was significantly different from 0 at 0.05; square symbols imply nonsignificant. In the *bottom row,* significance tests were not done so all symbols were round. *Left*: results for the entire period of the animal's use; *right*: the last 200 days. A steady re-training is apparent during this period. Also, the filled gray symbols represent a group of 5 new electrodes tested in 5 sequential sessions. With the exception of one point in the correlation plots, performance measures were high for these new electrodes.

rium and eventually stopped moving altogether. An emergency CT scan with infusion showed an enhancing fluid collection surrounding the dural graft above the electrode arrays. The purulent fluid was drained at the skull-cap interface. The neurological status of the monkey improved rapidly after this

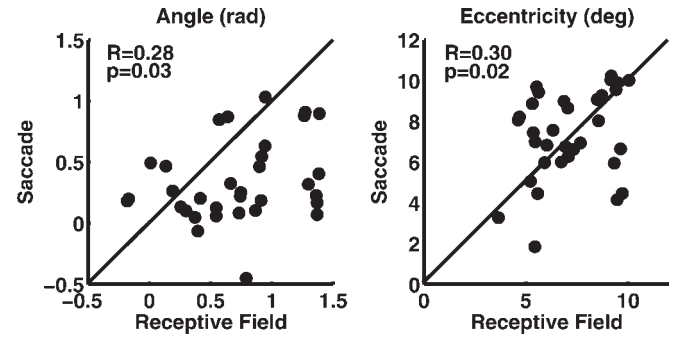

FIG. 10. Results for the 1st day the monkey was exposed to phosphenes, having previously been trained with visual targets. Units for angle are radians; units for eccentricity are degrees.

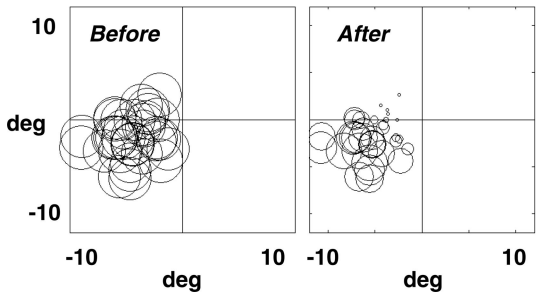

FIG. 11. Probable perifoveal visual deficit after subcranial trauma. The plots show results from a memory saccade task using visual targets. For each target location, the fraction of successful trials was expressed with a circle centered on the target. The circle's diameter is proportional to the fraction of successful saccades to target. Before trauma, most of the circles have a diameter of 1. After the trauma, performance in the task is lower overall, but this is especially clear near the fovea, where the monkey rarely made a saccade to the target.

drainage, implicating a significant mass effect as the most likely cause of the deterioration. Although the fluid contained multiple bacterial organisms, there was no clear evidence of generalized meningitis or sepsis, and the monkey was eventually able to resume visual testing after a 2-mo recovery period. The animal remained on daily antibiotics for the rest of his life.

Despite the animal's general recovery, he still showed signs of visual deficit; for example, when reaching to take treats he was frequently several centimeters off the mark. We did not thoroughly test his visual field; however, when visual targets were used as a means of retraining in the memory saccade task, some perifoveal visual impairment was obvious. In Fig. 11, the diameter of each circle is a measure of performance for saccades to the center of that circle. Large circles denote good performance. One readily sees that particularly near the fovea, performance was diminished.

In spite of this, the animal was able to retrain in the saccade-to-phosphene task (Fig. 9). But this was a tedious process. During fixation, the eyes drifted rapidly upward (Fig. 12) probably as a result of the visual impairment. Whatever the cause, the drift was such that the total gaze displacement was significant over the course of the 1-s stimulation period. Probably the phosphene appeared to move during this time, since this has been shown to occur in humans (Schmidt et al. 1996). However, because performance ultimately reached high levels (Fig. 9), we speculate that the animal learned to compensate for this apparent motion.

We tried to minimize the eye drift by reducing the stimulus duration to 200 ms, but this, unfortunately, only increased the rate of drift. We therefore decided not to prolong the experiment, which would normally have involved a gradual reduction in reward window sizes to determine the limits of saccade precision (scatter), and killed the animal instead in favor of the histological data.

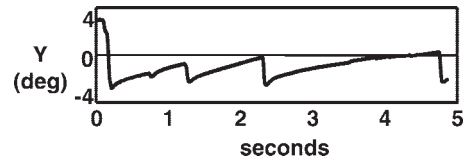

FIG. 12. Example of vertical eye position drift. The trace shows vertical eye position as a function of time. The monkey is supposed to be fixating a vertical position of 0. Unable to suppress the vertical drift, he has learned to start fixation below the target and saccade downward each time he reaches it.

Remapping receptive fields

Seven months after the array implantation, and after the occurrence and resolution of the epidural abscess, we remapped the channel receptive fields to determine whether they were still evident, and if so, whether they had moved. We tried flicker patterns and moving line patterns, as before, but found no evidence of receptive fields on any of the channels. Most of the channels were clearly registering cortical activity, but this activity was not modulated by visual stimuli. Not a single channel was able to meet the requirement stated in the preceding text for a receptive field, namely that responses to two adjacent locations have a z score >2. On inspection, the plots of neuronal activity versus (x, y) coordinates were devoid of any hint of a hotspot.

We do not know whether this disappearance of measurable receptive fields would have occurred without the trauma discussed in the preceding text. But, judging from Fig. 9, whatever caused the loss of visual response did not disrupt the ability of these channels to induce saccades to phosphenes.

Histology

Figure 13*A* shows the impression left in the cortex by the superstructure of one of the microelectrode clusters. In spite of the impression, all of the cortical layers are intact and do not appear remarkably different from those in the surrounding tissue. *B* shows the tip site of one of the short (0.7 mm) microelectrodes. The tip was in cortical layer 5, just shallow to the white matter underlying the cortex. Although the fixation of the cortex was not optimal, there were identifiable neurons within 20 μm of the tip site at the time the monkey was killed. *C* shows the tip site of one of the longer microelectrodes (1.3 mm) from the same array, which had passed through the stria of white matter and into the cortex of the subjacent gyrus.

Many of the HMRI clusters had depressed the cortex as illustrated in *A*. This behavior had rarely been observed with similar clusters implanted chronically in the sensorimotor cortex of cats (Liu et al. 1999). In this monkey, the clusters' subsidence may have been the result of mechanical pressure exerted by the epidural abscess, and it may account for the failure of the microelectrodes to record responses to visual stimuli following the occurrence and resolution of the epidural abscess. Forty-one microelectrode tip sites were located, and most (35) were within the cortex. In all cases in which the tips were within the cortex, there were neurons within 20 μm of the tip sites, as illustrated in *B* and *C*. The fact that most electrode tips were within cortex, combined with the fact that most channels continued to register cortical activity up to the end of the experiment (see previous text), suggests that the failure to detect visual responses was not the result of electrode tips residing in white matter. Instead, it may have been that the physiology of the cortex was altered by the intrusion of the clusters' superstructures.

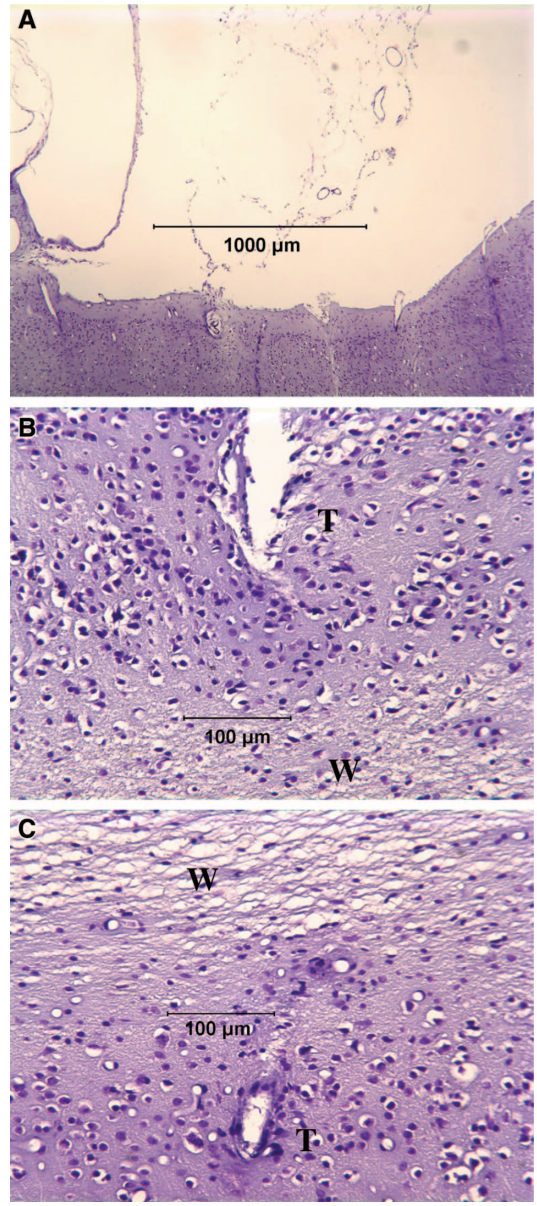

FIG. 13. *A*: low-power micrograph of a histologic section through the depression left by the superstructure of 1 of the HMRI clusters. The surface of the cortex has been depressed but the molecular layer (cortical layer 1) and the subjacent neurons appear to be intact. (Nissl stain). *B*: micrograph of the tip site (T) of 1 of the microelectrodes of the cluster shown in *A*. The tip site is within the deepest cortical layer, just dorsal to the underlying white matter (W). *C*: micrograph showing the tip site (T) of another microelectrode from the same cluster. This longer microelectrode had passed through the stria of white matter (W) and into the cortex of a subjacent gyrus.

DISCUSSION

We report on our efforts to establish an animal model for the development of an intracortical visual prosthesis. Our goal in this stage was to construct a large electrode array, implant it, and demonstrate its potential for use as a portal for information exchange through sensory cortex. We showed in our receptive field mapping tests that spatial information could be brought out through the array, and we showed in the saccade-to-phosphene task that spatial cues could be sent back in. We demonstrated that the monkey could map an array of electrical inputs to an array of saccade locations in much the same way he mapped visual inputs to saccade outputs, although the electrical task was substantially noisier.

In attaining these goals we worked out a variety of problems related to electrode electrochemistry, surgical technique, current delivery, and behavioral training. Our most important result is that the animal was able to perform an electrically stimulated spatial mapping task over many months with no

substantial performance degradation or histologically detectable damage around the electrode tips.

Saccade-to-phosphene task

The saccade-to-phosphene task was designed as a simple mechanism that would allow the monkey to take direct cortical stimulation as input and map it to an easily measurable output. The task has the advantages that it is reasonably easy to train, several thousand trials can be done in a day, and it has an exact visual counterpart that allows us to evaluate relative accuracy and precision.

A significant obstacle for us was the fact that receptive fields were largely confined to a $\sim 10 \times 10°$ area near the fovea. This is because of the limitations of placing electrodes only on the lateral aspect of the occipital cortex. We would have preferred to map a much larger portion of the visual field because it is difficult to analyze a spatial correlation over such a limited range. Nevertheless, within this region there was still a high correlation between saccade end points and receptive field locations once the trial-to-trial saccade scatter had been averaged out. This was evident after 2 wk of training, where correlation coefficients were >0.5 and highly significant and biases were close to 2°, and after a period of inactivity followed by retraining, where performance was similarly high (Fig. 9).

PERCEPTION OF PHOSPHENES VERSUS EMPIRICAL LEARNING. Let us postulate a cheater strategy where the monkey first identifies input from a particular channel by some nonvisual mechanism, perhaps via somatosensory innervation of the cortical vasculature; then, by trial and error, he learns that he is rewarded for saccading to a certain location after the activation of that channel. This process could simulate the results we obtained. And while it seems improbable given the large reward windows and the number of electrodes we were using, this possibility must still be ruled out.

Even on the first day of training, saccades were significantly correlated with receptive field locations (Fig. 10). Only three of these preliminary sessions were run; training then ceased for ~2 mo while we mapped receptive fields. Then, following a 2 wk period of training, the Period 2 data show fairly high correlations and very low biases (Fig. 9, *left*). Later, at the end of period 3, correlation coefficients were consistently close to 1, and thus substantially greater than the coefficients of approximately 0.3 obtained on the first day of training. Therefore one could argue that there is a weak innate ability to do the phosphene task, but the higher performance obtained with training involves cheating—empirical learning—that requires more time.

If this was true, the introduction of new channels that had never been activated before should bring the correlation (for those channels) down to ~0.3 again because there has been no time for empirical learning. On the contrary, we found performance for these electrodes to be as high as on any other channels at any other time. This suggests that there was indeed a learning process although not an empirical one where the monkey artificially mapped somatosensory shocks to memorized visual locations. We are referring instead to a learning process where the monkey became accustomed to mapping visually perceived flashes to saccade locations. The reason we allow ourselves to make the inference of a visual percept is because when the new electrode channels were introduced, the mechanism mapping them to the saccade output space was already in place. We can think of no other visuotopic cortical map that would exist prior to training.

SCATTER OF SACCADE END POINTS. Although the mean saccade end points were correlated with the receptive field locations, there was substantial scatter in saccades for stimulation on a given channel. Part of this is no doubt due to the nature of the task; namely, that saccading to the remembered location of a target is inherently less precise than saccading directly to a persistent target. But we also tested the monkey with visual targets in the same memory saccade task, and here the saccade dispersion was ~2.5 times smaller. Something about saccading to a remembered phosphene was more difficult than saccading to a remembered flash. This may have been in large part due to the difference in reward windows, which were typically 4–6° on a side for phosphenes and 0.25–2.5° on a side for visual targets. But other explanations cannot be ruled out.

It could be that the phosphenes were spatially diffuse and difficult to localize. We consider this unlikely. First, humans stimulated with intracortical electrodes using similar currents perceive point-like or nickel-sized images, not large, diffuse ones (Schmidt et al. 1996). Also, because the scatter of saccade end points in the phosphene task was roughly 2–3°, which is several times the size of V1 receptive fields at similar eccentricities, explaining the scatter in terms of diffuse neuronal activation would mean that current had to spread across several hypercolumns. But this is unlikely in view of experiments by Newsome and colleagues in extrastriate area MT (Murasugi et al. 1993). Using currents, like ours, on the order of 10–40 μA, they found that directionally specific effects could be elicited. Because a single MT column—roughly 1 mm, the size of a V1 hypercolumn—contains a complete set of direction columns, their currents were probably activating neurons at a distance considerably less than a millimeter. Moreover, they found that when electrodes were displaced by as little as 150 μm, effects changed profoundly. Their results suggest that stimulating currents of this magnitude probably do not activate neurons beyond roughly 100–200 μm, at least not sufficiently to have behavioral effects. Although results would not necessarily be the same in V1, the current spread in V1 would have to be orders of magnitude larger than in MT to explain the saccade scatter in terms of diffuse neuronal activation.

Another intriguing possibility is that phosphene locations, in contrast to visual locations, were not well stored during the memory phase of the task. Possibly, the unnatural manner in which the V1 neurons were activated precludes the efficient transfer of information into short-term storage.

LOSS OF VISUAL RESPONSIVENESS. As of 7 mo after implantation, we were unable to detect visual responses on any of the channels. This is consistent with the considerable degradation in the monkey's performance in the task requiring saccades to visual targets (Fig. 11). The histological data showed that at least many of the electrode clusters had sunk into the cortex, suggesting they were subjected to considerable mechanical pressure, possibly due to the large epidural abscess. This may have disrupted the normal physiology of the cortex and possibly affected subcortical components of the visual pathway as well. Nevertheless, the histology showed no obvious damage to

the cortical layers, and it is perhaps for this reason that microstimulation continued to be effective in the saccade-to-phosphene task.

V1 stimulation

HUMAN STUDIES. In 1918, Löwenstein and Borchardt reported that while performing an operation to remove bone fragments caused by a bullet wound, the patient's left occipital lobe was electrically stimulated, and the patient perceived flickering in the right visual field (Lowenstein and Borchardt 1918). Foerster (1929) and Krause (1924) reported similar cases of visual perception caused by electrical stimulation of visual cortex during removal an occipital epileptic focus. In studies by Penfield and colleagues (Penfield and Jasper 1954; Penfield and Rasmussen 1950), visual sensations, which they referred to as phosphenes, were evoked by stimulation of human occipital cortex. The visual sensations were described as stars, wheels, discs, spots, streaks, or lines. In a 1962 experiment by Button and Putnam (Button and Putnam 1962), four occipital-lobe electrodes with percutaneous wires were implanted each of three human subjects, with the wires connected to a crude apparatus that varied the electrical stimulus amplitude and frequency based on the output of a cadmium-sulfide photocell. The subjects were able to scan an area, holding the photocell in their hand, and grossly determine the location of illuminated objects.

The first attempt at chronic stimulation of human visual cortex was by Brindley and Lewin (1968), who implanted in a 52-year-old woman, a stimulation system consisting of 80 platinum electrode discs placed on the surface of the occipital pole. Eighty associated transcutaneously powered stimulators were placed over most of the surface of the right cortical hemisphere. Approximately 32 independent visual percepts were obtained, and Brindley carried out mapping studies and threshold measurements. Although some attempt was made to combine the phosphenes into crude letters and shapes, the implant did not prove to be of any practical use to the subject. Another subject received an implant in 1972 (Brindley et al. 1972). Of the 80 implanted electrodes, 79 produced visual percepts of varied size and shape.

Dobelle (Dobelle 2000; Dobelle and Mladejovsky 1974; Dobelle et al. 1974, 1976), Pollen (1975) and others continued to investigate the stimulation of human visual cortex through surface electrodes, using relatively large electrodes placed on the pia-arachnoid surface in individuals who were totally blind pursuant to lesions of the eyes or optic nerve. Dobelle et al. implanted at least three subjects with cortical surface arrays. They also tested the ability of the implanted subjects to use the perceptions produced by the electrodes to "read visual Braille" (Dobelle et al. 1976). Reading rates were considerably less that what could be obtained by tactile Braille.

In 1996, Schmidt et al. implanted a 42-yr-old woman, blind for 22 yr secondary to glaucoma, with 38 occipital intracortical electrodes (Schmidt et al. 1996). Intracortical as opposed to surface electrodes have exposed tip sizes of the same order of magnitude as cortical neurons, resulting in more precise control of neuronal function. Thirty-four electrodes initially produced spatial percepts with threshold currents in the range of 1.9–25 μA. Phosphene brightness could be modulated by varying stimulus amplitude, frequency, and pulse duration. The apparent size of phosphenes ranged from a pin-point to a nickel held at arm's length. At levels of stimulation near threshold, the phosphenes were often reported as having colors. As the stimulation level was increased, the phosphenes generally became white, gray, or yellowish. Electrodes spaced 500 μm apart generated separate phosphenes, but microelectrodes spaced 250 μm typically did not. This two-point resolution was about five times greater than had previously been achieved with electrodes on the surface of the cortex.

ANIMAL STUDIES. The earliest documented stimulation of striate cortex in monkeys goes back to Schafer, who found that eye movements could be elicited by electrically stimulating V1 (Schafer 1888). These were later shown by Schiller to be saccadic (Schiller 1972). Doty performed extensive microstimulation studies in macaque V1 (Doty 1965). He demonstrated that monkeys could not only discriminate stimulation at different cortical sites; they could in fact discriminate stimulation at different frequencies, even when currents were matched, and they could discriminate the polarity of current flow. These findings suggest the potential for fine manipulation of visual percepts through the control of current parameters on a given electrode.

DeYoe systematically studied current detection thresholds in macaque V1 as a function of various stimulation parameters (DeYoe 1983). The lowest thresholds were achieved with cathodal, constant current trains of 30 200-μs pulses delivered at 100 Hz. These thresholds strongly depended on the depth of stimulation: for lower layer 3/upper layer 4 and upper layer 5, current detection thresholds were 1–5 μA, whereas in other layers, thresholds were significantly higher.

Tehovnik, Schiller, and colleagues have developed a paradigm that allows them to precisely quantify certain behavioral effects of stimulation in V1. The task involves saccades to a visual target interspersed with saccades to a stimulation-induced target. The authors studied current thresholds, saccade latencies, and chronaxies (time constants of neural elements) at various cortical depths (Tehovnik et al. 2003). All three response parameters varied as a function of depth; in general, current thresholds were lower, and latencies and chronaxies were shorter, in the deepest layers of cortex. This need not be taken as a contrast to the DeYoe results; because the deep layers of V1 send direct projects to the superior colliculus (Fries 1984), this could explain why the saccade-based task was more efficient with deep stimulation.

Improvements to the prosthesis

In the weeks after the implantation of the electrodes and head hardware, several issues emerged relative to the reliability of the head-mounted connector housings. The housings were fabricated from polycarbonate using helicoils to reinforce the threads of the screw holes that accepted the screws from the housing lids. These holes extended vertically from the top of the housing to the lower edge, which sat on the skull, providing a channel for fluid to emerge from the screw holes and creating a difficult maintenance problem for keeping the O-ring gasketed lid sealed. After a couple of weeks bases of the holes were sealed from the top, under a microscope, using a silicone adhesive.

Maintenance of the polycarbonate housings was often difficult. To maintain a sealed lid, excessive tightening pressure

was needed on the lid screws to keep the O-ring compressed, and this caused failure of the threads even with the helicoils. Soon after implantation we changed from an O-ring to a soft silicone rubber pad, and this eliminated the lead sealing problem. Sometimes the animal would cause damage to the housing by hitting his head against the cage.

In the region above the implanted electrodes, the failure of the removed bone flap to reincorporate into the surrounding skull, combined with the presence of the foreign acrylic material, exacerbated the problem of tracking infections. Numerous channels existed along the edges of the acrylic leading to the electrode implantation site. The edge of the scalp surrounding the acrylic skull cap was chronically prone to low levels of infection and bacterial growth. This eventually resulted in the abscess that formed in the epidural space.

Because this first implantation experience, we have redesigned both the head hardware and the surgical procedure. The connector housings are now fabricated from titanium, making them more rugged and less susceptible to mechanical damage as well as increasing their biocompatibility. Rather than mounting the connector housings directly to the skull, we first install a titanium baseplate that is anchored to the skull using a combination of self-tapping surgical screws and surgical-grade cranioplasty. The amount of cranioplasty is minimized, using only enough to ensure attachment of the baseplate to the skull. The baseplate has pretapped 0–80 screw holes that accept screws from the connector housing, thus facilitating the installation of the housing and the delicate electrode arrays. The craniotomy is now accomplished so that the bone flap can be replaced over the implanted electrodes using titanium attachment plates. A piece of harvested fascia is used to cover the bone flap. The scalp is now closed so that it contacts the connector housing. This is facilitated by making the connector housing in a boat-like shape.

In recent experiences with this modified surgical procedure, we have seen a rapid seal develop between the connector housing and the scalp. Over approximately a 2-mo period, the scalp then naturally recedes to the smooth junction of the cranioplasty and the underlying skull. The recession of the scalp stops at this point, producing an edge of healthy tissue that is well adhered to the underlying skull. Little or no fluid leakage at the edge of the scalp is seen on a daily basis, and there are no signs of infection. It is our feeling that this surgical animal model is now mature, and we are proceeding with new psychophysical experiments on an animal recently implanted with 96 electrodes.

One of the most pressing issues for the development of a cortical prosthesis is the problem of safely injecting sufficient charge into the neural tissue to assure neuronal stimulation. The transfer of charge from the metal electrode to the extracellular fluid relies on oxidation-reduction (redox) reactions at the electrode-fluid interface. The specific chemistry depends on the type of electrode; with platinum, for example, charge is carried by protons adherent to the electrode surface, while iridium oxide supports a redox reaction within a porous hydrated film. But for all metals, there is a limited supply of chemical species for carrying charge; when these are depleted, the electrode voltage must swing high to maintain the same current, and typically the current is then carried by the oxidation and reduction of water. This produces H_2 and O_2 gas, which may damage surrounding tissue and may destroy the electrode itself. Other damaging redox products may be formed and diffuse into the tissue when electrode voltage excursions are large.

We recently made cyclic voltammetry (CV) measurements on iridium oxide electrodes chronically implanted in a rhesus monkey. CV measures the water window, the amount of charge that can be injected within a voltage range safe from hydrolysis. After only 2 mo of implantation, we were surprised to find that these electrodes (which had not be previously stimulated) retained only a fraction of the charge capacity they had before implantation. This may have been due to coating of the electrodes by glial tissue.

We are currently testing various protocols for conditioning implanted microelectrodes for restoration and maintenance of the electrode charge capacity. Two additional goals in our animal tests will be to find the minimum currents effective in behavioral control and to find optimal waveforms in terms of maximizing charge capacity for a given behavioral effect. Before genuinely long-term implants are feasible in humans, it will be necessary to guarantee an electrode and a system for driving it and perhaps conditioning it in vivo, such that it remains effective for the duration of the implant.

Future experiments

To simulate natural vision, it will eventually be necessary to stimulate many cortical sites in parallel. Nothing we know currently about microstimulation justifies the assumption that multiple inputs will be perceptually combined in any meaningful way. Possibly, the key to multi-site stimulation lies in the distribution of pulses on the individual electrodes—for instance, pulses distributed over time as Poisson rather than periodic sequences. In any case, experiments will need to be designed in such a way as to evaluate the effectiveness with which the brain integrates input at multiple sites. For example, monkeys could be trained to distinguish simple shapes, sketched by patterns of stimulation in an array, or to judge motion or orientation where the signal is weak at each electrode but probabilistically strong when considered over all electrodes. Once a task is established that requires the animal to integrate signals from multiple electrodes, one can begin to experiment with different patterns of current delivery on the individual electrodes to see which patterns are best integrated by the animal in performing the task.

Summary

It is our goal to develop visual prosthesis technology through systematic research, starting with the most basic problems and working methodically toward a practical device. We expect the immediate application of this prosthesis to be in basic visual science with clinical benefits being realized later.

This paper documents our studies with the largest intracortical stimulating array ever implanted. We showed that a monkey could be trained in a nontrivial task requiring him to map cortical stimulation to saccade endpoints and that his performance in this task did not degrade, on the whole, over the course of many months. The importance of this is to suggest that rather aggressive testing is possible in the macaque, and this opens the door to what we hope will be a multitude of basic-research efforts to understand the feasibility and mech-

anisms of communication with visual cortex through a brain-machine interface.

ACKNOWLEDGMENTS

We are grateful to E. DeYoe, W. Newsome, L. Optican, G. Purushothaman, B. Richmond, and R. Wurtz for advice and to C. Wardrip and S. Santhakumar for technical assistance.

GRANTS

This work was supported by National Institute of Neurological Disorders and Stroke Grant NS-40690-01A1, the Brain Research Foundation, the Pritzker-Galvin Challenge Fund, and private donations.

REFERENCES

Bak M, Girvin JP, Hambrecht FT, Kufta CV, Loeb GE, and Schmidt EM. Visual sensations produced by intracortical microstimulation of the human occipital cortex. *Med Biol Eng Comput* 28: 257–259, 1990.

Brindley GS, Donaldson PE, Falconer MA, and Rushton DN. The extent of the region of occipital cortex that when stimulated gives phosphenes fixed in the visual field. *J Physiol* 225: 57P–58P, 1972.

Brindley GS and Lewin WS. The sensations produced by electrical stimulation of the visual cortex. *J Physiol* 196: 479–493, 1968.

Button J and Putnam T. Visual responses to cortical stimulation in the blind. *J Iowa Med Soc LII* 1: 1–21, 1962.

DeYoe EA. *An Investigation in the Awake Macaque of the Threshold for Detection of Electrical Currents Applied to Striate Cortex: Psychophysical Properties and Laminar Differences* (PhD thesis) Rochester, NY: University of Rochester, 1983.

Dobelle WH. Artificial vision for the blind by connecting a television camera to the visual cortex. *ASAIO J* 46: 3–9, 2000.

Dobelle WH and Mladejovsky MG. Phosphenes produced by electrical stimulation of human occipital cortex, and their application to the development of a prosthesis for the blind. *J Physiol* 243: 553–576, 1974.

Dobelle WH, Mladejovsky MG, Evans JR, Roberts TS, and Girvin JP. "Braille" reading by a blind volunteer by visual cortex stimulation. *Nature* 259: 111–112, 1976.

Dobelle WH, Mladejovsky MG, and Girvin JP. Artifical vision for the blind: electrical stimulation of visual cortex offers hope for a functional prosthesis. *Science* 183: 440–444, 1974.

Doty RW. Conditioned reflexes elicited by electrical stimulation of the brain in macaques. *J Neurophysiol* 28: 623–640, 1965.

Ferree JW. *Estimated Statistics on Blindness and Vision Problems.* New York: The National Society for the Prevention of Blindness, 1966.

Foerster O. Beitrage zur Pathophysiologie der Sehspare. *J Psychol Neurol* 39: 463–485, 1929.

Fries W. Cortical projections to the superior colliculus in the macaque monkey: a retrograde study using horseradish peroxidase. *J Comp Neurol* 230: 55–76, 1984.

Hubel DH and Wiesel TN. Receptive fields and functional architecture of monkey striate cortex. *J Physiol* 195: 215–243, 1968.

Krause F. Die Sehbahnen in chirurgischer Beziehung und die faradische Reizung des Sehzentrums. *Klin Wochenschr* 3: 1260–1265, 1924.

Liu X, McCreery DB, Carter RR, Bullara LA, Yuen TG, and Agnew WF. Stability of the interface between neural tissue and chronically implanted intracortical microelectrodes. *IEEE Trans Rehabil Eng* 7: 315–326, 1999.

Lowenstein K and Borchardt M. *Dtsch Z Nervenheilk* 58: 264–292, 1918.

Murasugi CM, Salzman CD, and Newsome WT. Microstimulation in visual area MT: effects of varying pulse amplitude and frequency. *J Neurosci* 13: 1719–1729, 1993.

Penfield W and Jasper H. *Epilepsy and the Functional Anatomy of the Human Brain.* London: Churchill, 1954, p. 116–126.

Penfield W and Rasmussen T. *The Cerebral Cortex in Man.* New York: MacMillan, 1950.

Pollen DA. Some perceptual effects of electrical stimulation of the visual cortex in man. In: *The Nervous System*, edited by Tower DB. New York: Raven, 1975, p. 519–528.

Schafer EA. Experiments on the electrical excitation of the cerebral cortex in the monkey. *Brain* 11: 1–6, 1888.

Schiller PH. The role of the monkey superior colliculus in eye movement and vision. *Invest Ophthalmol* 11: 451–460, 1972.

Schmidt EM, Bak MJ, Hambrecht FT, Kufta CV, O'Rourke DK, and Vallabhanath P. Feasibility of a visual prosthesis for the blind based on intracortical microstimulation of the visual cortex. *Brain* 119: 507–522, 1996.

Tehovnik EJ, Slocum WM, and Schiller PH. Saccadic eye movements evoked by microstimulation of striate cortex. *Eur J Neurosci* 17: 870–878, 2003.

Troyk P, Bak M, Berg J, D B, Cogan S, Erickson R, Kufta C, McCreery D, Schmidt E, and Towle V. A model for intracortical visual prosthesis research. *Artif Organs* 27: 1005–1015, 2003.